ChemComm

COMMUNICATION

View Article Online
View Journal | View Issue

Cite this: *Chem. Commun.*, 2014, **50**, 3806

Received 18th December 2013,
Accepted 14th February 2014

DOI: 10.1039/c3cc49571j

www.rsc.org/chemcomm

Heme bound amylin self-assembled monolayers on an Au electrode: an efficient bio-electrode for O_2 reduction to H_2O†

Kushal Sengupta, Sudipta Chatterjee, Soumya Mukherjee, Somdatta Ghosh Dey* and Abhishek Dey*

Self-assembled monolayers of the water soluble hydrophilic part of naturally occurring amylin and its Arg11 mutant have been assembled on an Au surface, which are found to efficiently catalyze selective $4e^-/4H^+$ O_2 reduction reaction (ORR) upon binding heme with a k_{cat} of $\sim 10^7$ M^{-1} s^{-1} under ambient conditions, where the Arg11 residue plays the key role of proton transfer in determining the rate of ORR.

Electrochemical reduction of O_2 to H_2O with high catalytic rates and turnover numbers has significant implications in biofuel cells, bio-sensors, *etc.*[1–3] While precious metals and metal-alloy based O_2 reduction reaction (ORR) catalysts have been found to be promising candidates, their utility is limited by their high costs.[3] Metallo-porphyrins and metallo-corroles are reported to function as good ORR electrocatalysts.[4–9] In these cases the involvement of partially reduced oxygen species (PROS) has proved to be detrimental for the long term stability of these catalysts.[4,10] Prior investigations have revealed that naturally occurring enzymes like laccases, immobilized directly on electrodes, reduce O_2 at reasonable catalytic rates.[11–13] The advantage of using a natural scaffold has been widely discussed and demonstrated in non-heme iron proteins,[14,15] electron transport proteins,[16–18] oxidases[19,20] and, recently, in hydrogenases.[21] Hence a naturally occurring protein/peptides scaffold, which can bind heme and can be easily attached to electrodes, could form a potential biochemical scaffold for heme based ORR catalysts.

Amylin (Ay) or the human islet amyloid polypeptide protein is a principal constituent of fibrillar amyloid deposits observed in patients suffering from type 2 diabetes mellitus. It comprises of 37 amino-acid residues (1–37) and is found in blood.[22,23] Recent studies establish that the non-amyloidogenic segments 1–19 is the heme binding domain where a single heme is bound by the His18 residue.[24] Arg11, though not directly bound to heme, plays a key role by providing hydrogen bonding interactions with the propionate side chain of heme.[24] Two cysteine residues (Cys2 and Cys7) present in the 1–19 domain do not bind heme[24] and are thus available to bind to the Au(111) surface, as observed for other Cys appended peptides.[25,26] Here, we report the formation of a self-assembled monolayer (SAM) of Ay (1–19) on the Au surface (Ay_{SAM}) which when bound to heme acts as an excellent bio-electrode for O_2 reduction. Heme bound to Ay_{SAM} (WT) and Arg11Asn mutant (Ay_{SAM}-R11N) show $4e^-/4H^+$ O_2 reduction with minimal PROS formation having rates as high as 10^7 M^{-1} s^{-1}, which is several orders of magnitude greater than most of the reported metallo-porphyrin and metallo-enzyme based electrocatalysts.[11,27]

The cysteine residues present in Ay (1–19) bearing either a thiol group or a disulfide bridge are used to form a monolayer on Au electrodes. Clean Au surfaces upon being immersed in a 0.1 mM solution of Ay (1–19) show the presence of small and isolated features (Fig. 1A). These features have a height distribution of 3–5 nm (Fig. 1B). Very few clusters ranging from 6 to 7 nm are also seen, which are randomly distributed. Unlike previous reports of amyloid β peptides (associated with Alzheimer's disease),[26] these Ay_{SAM} surfaces do not show large structures resulting from peptide aggregation.[28] Ay (1–19) has 19 residues and considering a 3.2 Å translation per residue, an upright Ay peptide should have a height of ~60 Å (6 nm). This is more than the observed height of 3–5 nm. Alternatively, assuming the segments 1–7 runs parallel

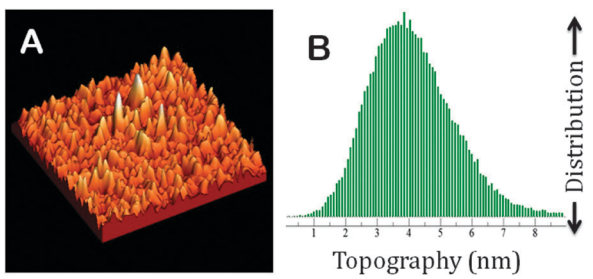

Fig. 1 (A) 3D topology AFM image of the amylin (1–19) modified Au surface (Ay_{SAM}). (B) Height distribution profile diagram of the corresponding surface.

Department of Inorganic Chemistry, Indian Association for the Cultivation of Science, 2A & 2B Raja S. C. Mullick Road, Jadavpur, Kolkata, 700032, India.
E-mail: icad@iacs.res.in, icsgd@iacs.res.in

† Electronic supplementary information (ESI) available: Experimental detials, AFM, CV, SERRS, and BE data. See DOI: 10.1039/c3cc49571j

to the electrode, anchored by Cys2 and Cys7 at the ends, and the remaining 12 residues (8–19) project out of the surface, an approximate height of 4 nm (3.2 × 12 Å) can be estimated for such a construct consistent with the observed height of 4 ± 1 nm in the AFM data (Fig. 1). Note that similar results were observed in the AFM images of the Ay_{SAM}-R11N (Fig. S2, ESI†).[29]

Ay_{SAM} formation on the Au electrode surfaces shields the electrode and abolishes the electrocatalytic O_2 reduction catalyzed by bare Au electrodes (Fig. S3, ESI†). For further insulation of these modified surfaces from the solution phase, the Ay_{SAM} covered surfaces were immersed in octanethiol solution which led to further decrease in the capacitive current (Fig. S3, ESI†). Heme binding to Ay_{SAM} is characterized using Surface Enhanced Resonance Raman Spectroscopy (SERRS).[30,31] SERRS data of heme–Ay_{SAM} show the ν_4, ν_3 and the ν_2 bands at 1370 cm^{-1}, 1489 cm^{-1} and 1569 cm^{-1} respectively, indicating the presence of a six coordinate (6C) Fe^{III} high-spin (HS) species on the surface (Fig. 2A, red).[32,33] Careful fitting of the ν_2 band shows the presence of a 6C Fe^{III} low-spin (LS) component having the ν_2 band at 1586 cm^{-1} (Fig. S4, ESI†). Note that these values are in good agreement with those obtained for heme–Ay complexes in solution.[24] In the presence of imidazole the ν_4, ν_3 and ν_2 bands of heme–Ay_{SAM} shift to 1374 cm^{-1}, 1505 cm^{-1} and 1585 cm^{-1} respectively, indicating the conversion of the HS species to a pure 6C Fe^{III} LS species (Fig. 2A, blue) and suggesting the presence of an exchangeable ligand (likely to be H_2O) in the heme–Ay_{SAM} complex.[32,33] Note that the structural organization of the heme bound Ay_{SAM}-R11N SAM is similar to that of the WT (SERRS, absorption and capacitance data; Fig. S5–S7, ESI†).

Cyclic voltammetry (CV) of heme–Ay_{SAM} (WT) in degassed pH 7 buffer under anaerobic conditions shows a well developed quasi-reversible Fe^{III}/Fe^{II} process at −108 mV *vs.* NHE (Fig. 2B, red; Fig. S8, ESI†). The Ay_{SAM}-R11N mutant shows the $Fe^{III/II}$ redox couple at −120 mV (Fig. 2B, green). The surface coverages were measured from the area under the oxidation and reduction waves and were found to be 9.8 × 10^{12} molecules cm^{-2} and 2.0 × 10^{13} molecules cm^{-2} for WT and R11N mutant, respectively (Table 1). Such low

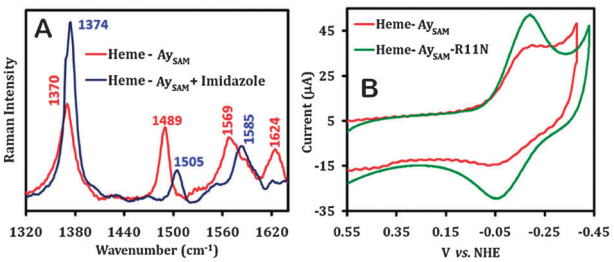

Fig. 2 (A) SERRS data of heme–Ay_{SAM} in pH 7 buffer (red) and in the presence of 100 mM imidazole in pH 7 (blue), collected under resting (oxidizing) conditions. (B) CV data of heme–Ay_{SAM} (red) and heme–Ay_{SAM}-R11N mutant (green) in deoxygenated pH 7 buffer at a scan rate of 1 V s^{-1}.

Table 1 Electrochemical response of heme–Ay_{SAM}

Species	$\Gamma_{catalyst}$ (molcules cm^{-2})	n	PROS (%)	k_{cat} (M^{-1} s^{-1})
Heme–Ay_{SAM}	~9.8 × 10^{12}	4	9 ± 0.5	(1.8 ± 0.6) × 10^7
Heme–Ay_{SAM}-R11N	~2 × 10^{13}	4	6.6 ± 1.0	(2.7 ± 0.4) × 10^5

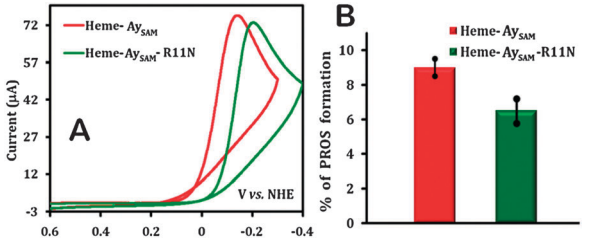

Fig. 3 (A) CV data of heme–Ay_{SAM} (red) and heme–Ay_{SAM}-R11N mutant (green) obtained in air saturated pH 7 buffer at a scan rate of 50 mV s^{-1}. (B) Bar diagram representation of the amount of PROS produced by the respective heme bound species.

surface coverage suggests formation of a monolayer of site isolated heme–Ay_{SAM} active sites. Multi-layers formed from physiadsorption have coverages $>10^{14}$ molecules cm^{-2}.[34] In aerated buffer solutions, CV of heme–Ay_{SAM} in the pH 7 buffer shows an electrocatalytic O_2 reduction current peaking at −150 mV (Fig. 3A, red). Similar results are also observed in the R11N mutant. The potential for O_2 reduction is ~30 mV lower in the R11N mutant, consistent with the lower $Fe^{III/II}$ potential observed in this mutant relative to the WT. Rotating ring disc electrochemistry (RRDE) is used to estimate the amount of PROS, formed due to incomplete reduction of O_2.[35] In this technique any O_2^{2-}, *i.e.*, a $2e^-$ reduction product of O_2, produced in the modified Au disc electrode is radially diffused to the encircling Pt ring, which is held at a potential where the H_2O_2 is oxidized back to O_2. The amount of PROS produced by heme–Ay_{SAM} is about 9 ± 0.5% while for the R11N mutant the amount of PROS produced is 6.6 ± 1% (Fig. 3B and Fig. S9, ESI†).[36] The decrease in PROS when the Arg11 residue is mutated to Asn indicates that the acidic Arg11 residue, even if not directly involved in heme binding, is likely involved in 2nd sphere interaction with the active site, consistent with previous reports.[26,37,38] Such interaction may provide efficient proton transfer pathways into the active site (*vide infra*).

Electrocatalytic O_2 reductions of these species are further investigated using a rotating disc electrode (RDE). Linear Sweep Voltammetry (LSV) of heme–Ay_{SAM} and the corresponding mutant show a substrate diffusion limited catalytic O_2 reduction current below −200 mV (Fig. 4A and B). The O_2 reduction current increases with increasing rotation rates following the Koutecky–Levich equation, $i^{-1} = i_K(E)^{-1} + i_L{}^{-1}$, where $i_K(E)$ is the potential dependent kinetic current expressed as $nFA[O_2]k_{cat}\Gamma_{catalyst}$, and i_L is the Levich current. i_L is expressed as $0.62nFA[O_2](D_{O_2})^{2/3}\omega^{1/2}\nu^{-1/6}$, where n is the number of electrons transferred to the substrate, F is the faraday constant, A is the macroscopic area of the disc (0.192 cm^2), $[O_2]$ is the concentration of O_2 in an air saturated buffer (0.2 mM) at 25 °C, k_{cat} is the 2nd order rate of catalytic O_2 reduction, $\Gamma_{catalyst}$ is the catalyst concentration in moles cm^{-2}, D_{O_2} is the diffusion coefficient of O_2 (2.2 × 10^{-5} cm^2 s^{-1}) at 25 °C, ω is the angular velocity of the disc and ν is the kinematic viscosity of the solution (0.009 cm^2 s^{-1}) at 25 °C.[35] The plot of i^{-1} at multiple rotation rates *vs.* the inverse square root of the angular rotation rate ($\omega^{-1/2}$) is linear. The number of electrons (n) involved in the O_2 reduction by a catalytic species may be calculated from the slope and 2nd order rate of catalysis (k_{cat}) from the intercept of this linear plot. The slopes obtained from the experimental data, at different potentials in the substrate diffusion

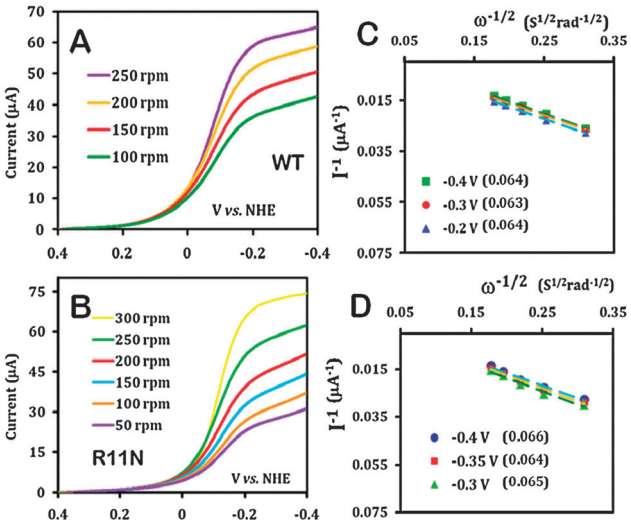

Fig. 4 RDE plots of heme–Ay_{SAM} (A) and heme–Ay_{SAM}-R11N (B), in air saturated pH 7 buffer at a scan rate of 50 mV s^{-1} at multiple rotations. (C) and (D) are the respective K–L plots of these species (given in coloured line) at different potentials. The values in parentheses are the respective slope values (μA^{-1} $s^{-1/2}$ $rad^{1/2}$). Theoretical $4e^-$ slope is 0.062 μA^{-1} $s^{-1/2}$ $rad^{1/2}$.

controlled region, for heme–Ay_{SAM} and the R11N mutant species are identical to the theoretical slope predicted for a $4e^-$ process (Fig. 4C and D, Table 1). This is consistent with the RRDE data which showed more than 90% $4e^-/4H^+$ reduction of O_2 to H_2O.

The intercept of the K–L plot can be used to estimate the k_{cat} ($i_k = nFA[O_2]k_{cat}\Gamma_{catalyst}$) for the $4e^-/4H^+$ ORR, catalyzed by the heme bound peptides. The k_{cat} values, obtained from the K–L plots at −0.4 V *vs.* NHE, of heme–Ay_{SAM} and heme–Ay_{SAM}-R11N are estimated to be $(1.8 \pm 0.6) \times 10^7$ M^{-1} s^{-1} and $(2.7 \pm 0.4) \times 10^5$ M^{-1} s^{-1}, respectively (Table 1). The k_{cat} for O_2 reduction by native heme–Ay_{SAM} is at least two orders of magnitude greater than the values reported for other metallo-porphyrin based electrocatalysts.[27] The role of the Arg11 residue is clearly demonstrated by the fact that the catalytic rate of the R11N mutant is two orders of magnitude lower than that of the WT peptide. It is likely that the Arg11 residue provides a proton transfer channel to the active site which is essential for O_2 reduction to H_2O.[37,38] The ORR current has a Tafel slope of ∼120 mV per decadoic increase in current (Fig. S11A, ESI†) consistent with previous reports.[39] Bulk electrolysis (BE) experiment with heme–Ay_{SAM} at −250 mV in pH 7 shows that the catalyst is stable for at least 5000 s and in this period it consumes a charge of 0.085 C (Fig. S11B, ESI†).[40] Thus the turnover number (TON) of the heme–Ay_{SAM} catalyst is determined to be $>10^4$. While k_{cat} of ORR has been determined using RDE for several synthetic metalloporphyrin catalysts absorbed on electrodes (*i.e.*, multilayers), k_{cat} could not be determined for a monolayer of catalyst, thus far, due to their inherent instability.[4,41,42] However the current construct, where the Ay peptide is attached to the Au electrode *via* two Cys–Au linkages, yields a very stable monolayer and allows determination of k_{cat} of ORR, using RDE, by a monolayer of a metallo-porphyrin electrocatalyst.[43] The stability of this construct is also reflected in the BE experiments.

In summary, it has been shown that naturally occurring Ay peptides spontaneously assemble on Au electrodes using the thiol group of Cys2 and Cys7 residues. The Ay_{SAM} assemblies on Au electrodes bind heme and can be characterized using SERRS and CV. The resultant heme–Ay_{SAM} complex on the electrode is very stable and can catalyze ORR at a rate of 10^7 M^{-1} s^{-1}, which is 100 times faster than any man-made metalloporphyrin catalyst reported so far. The facile ORR by the WT heme–Ay_{SAM} complexes is due to the presence of Arg11 residue in the active site, which likely provides a facile H^+ transfer pathway. A facile proton transfer pathway has been identified as a key factor for an efficient ORR in both natural and artificial systems.[9,44,45]

We thank the SERC Fast Track Scheme SR/FT/CS-34/2010 (SGD) and SR/S1/IC-35/2009 (AD), Department of Science and Technology, Govt. of India for funding this research. K.S., S.C. and S.M. thank CSIR, India, for Senior (K.S. and S.C.) and Junior (S.M.) Research Fellowships.

Notes and references

1 S. Calabrese Barton, J. Gallaway and P. Atanassov, *Chem. Rev.*, 2004, **104**, 4867.
2 J. A. Cracknell, K. A. Vincent and F. A. Armstrong, *Chem. Rev.*, 2008, **108**, 2439.
3 A. A. Gewirth and M. S. Thorum, *Inorg. Chem.*, 2010, **49**, 3557.
4 J. P. Collman, N. K. Devaraj, R. A. Decreau, Y. Yang, Y.-L. Yan, W. Ebina, T. A. Eberspacher and C. E. D. Chidsey, *Science*, 2007, **315**, 1565.
5 C. J. Chang, Z.-H. Loh, C. Shi, F. C. Anson and D. G. Nocera, *J. Am. Chem. Soc.*, 2004, **126**, 10013.
6 A. Hosseini, C. J. Barile, A. Devadoss, T. A. Eberspacher, R. A. Decreau and J. P. Collman, *J. Am. Chem. Soc.*, 2011, **133**, 11100.
7 Z. Ou, A. Lu, D. Meng, S. Huang, Y. Fang, G. Lu and K. M. Kadish, *Inorg. Chem.*, 2012, **51**, 8890.
8 A. Schechter, M. Stanevsky, A. Mahammed and Z. Gross, *Inorg. Chem.*, 2012, **51**, 22.
9 C. T. Carver, B. D. Matson and J. M. Mayer, *J. Am. Chem. Soc.*, 2012, **134**, 5444.
10 J. P. Collman, R. A. Decreau, H. Lin, A. Hosseini, Y. Yang, A. Dey and T. A. Eberspacher, *Proc. Natl. Acad. Sci. U. S. A.*, 2009, **106**, 7320.
11 N. S. Parimi, Y. Umasankar, P. Atanassov and R. P. Ramasamy, *ACS Catal.*, 2012, **2**, 38.
12 P. Olejnik, B. Palys, A. Kowalczyk and A. M. Nowicka, *J. Phys. Chem. C*, 2012, **116**, 25911.
13 C. F. Blanford, R. S. Heath and F. A. Armstrong, *Chem. Commun.*, 2007, 1710.
14 R. B. Hill, D. P. Raleigh, A. Lombardi and W. F. DeGrado, *Acc. Chem. Res.*, 2000, **33**, 745.
15 E. G. Kovaleva, M. B. Neibergall, S. Chakrabarty and J. D. Lipscomb, *Acc. Chem. Res.*, 2007, **40**, 475.
16 T. D. Wilson, Y. Yu and Y. Lu, *Coord. Chem. Rev.*, 2013, **257**, 260.
17 A. Osyczka, C. C. Moser, F. Daldal and P. L. Dutton, *Nature*, 2004, **427**, 607.
18 C. J. Reedy and B. R. Gibney, *Chem. Rev.*, 2004, **104**, 617.
19 N. Yeung, Y.-W. Lin, Y.-G. Gao, X. Zhao, B. S. Russell, L. Lei, K. D. Miner, H. Robinson and Y. Lu, *Nature*, 2009, **462**, 1079.
20 J. A. Sigman, H. K. Kim, X. Zhao, J. R. Carey and Y. Lu, *Proc. Natl. Acad. Sci. U. S. A.*, 2003, **100**, 3629.
21 G. Berggren, A. Adamska, C. Lambertz, T. R. Simmons, J. Esselborn, M. Atta, S. Gambarelli, J. M. Mouesca, E. Reijerse, W. Lubitz, T. Happe, V. Artero and M. Fontecave, *Nature*, 2013, **499**, 66.
22 P. Westermark, C. Wernstedt, E. Wilander, D. W. Hayden, T. D. O'Brien and K. H. Johnson, *Proc. Natl. Acad. Sci. U. S. A.*, 1987, **84**, 3881.
23 G. J. Cooper, A. C. Willis, A. Clark, R. C. Turner, R. B. Sim and K. B. Reid, *Proc. Natl. Acad. Sci. U. S. A.*, 1987, **84**, 8628.
24 S. Mukherjee and S. G. Dey, *Inorg. Chem.*, 2013, **52**, 5226.
25 S. Terrettaz, W.-P. Ulrich, H. Vogel, Q. Hong, L. G. Dover and J. H. Lakey, *Protein Sci.*, 2002, **11**, 1917.
26 D. Pramanik, K. Sengupta, S. Mukherjee, S. G. Dey and A. Dey, *J. Am. Chem. Soc.*, 2012, **134**, 12180.
27 R. Boulatov, J. P. Collman, I. M. Shiryaeva and C. J. Sunderland, *J. Am. Chem. Soc.*, 2002, **124**, 11923.

28 Note that even after incubating the Au surface in AySAM solution for a few months no aggregation is observed (Fig. S1, ESI†).
29 Note that the diluent C_8SH SAM is only $\sim$2 nm. Thus the major segment of the Ay peptide projects into the aqueous phase which allows access to protons (from H_2O) required for ORR.
30 D. H. Murgida and P. Hildebrandt, *Acc. Chem. Res.*, 2004, **37**, 854.
31 K. Sengupta, S. Chatterjee, S. Samanta and A. Dey, *Proc. Natl. Acad. Sci. U. S. A.*, 2013, **110**, 8431.
32 G. Rakshit and T. G. Spiro, *Biochemistry*, 1974, **13**, 5317.
33 T. G. Spiro and J. M. Burke, *J. Am. Chem. Soc.*, 1976, **98**, 5482.
34 A. Bettelheim, R. J. H. Chan and T. Kuwana, *J. Electroanal. Chem. Interfacial Electrochem.*, 1980, **110**, 93.
35 A. J. Bard and L. R. Faulkner, *Electrochemical Methods: Fundamentals and Applications*, J Wiley & Sons, New York, 2001.
36 Simple hemin physiabsorbed on C_8SH SAM yields about 23 $\pm$ 1% of PROS (Fig. S10, ESI†).
37 D. R. Menick, N. Carrasco, L. Antes, L. Patel and H. R. Kaback, *Biochemistry*, 1987, **26**, 6638.
38 B. O. Krogh and S. Shuman, *J. Biol. Chem.*, 2002, **277**, 5711.
39 C. Shi and F. C. Anson, *Electrochim. Acta*, 1994, **39**, 1613.
40 Note that similar BE experiments with heme–Ay_{SAM}-R11N shows that the catalyst is not stable after about 300 s, indicating that Arg11 plays a key role in its stability (Fig. S11, ESI†).
41 J. P. Collman and R. A. Decreau, *Chem. Commun.*, 2008, 5065.
42 Most monolayers of catalysts (resulting from covalent attachment of the catalyst to the SAM) are tethered to the electrode using single Au–S linkage. These constructs are possibly not stable to perform K–L analysis because of the hydrodynamic friction caused by the rotation of the electrode during an RDE experiment.
43 Note that RDE experiments with simple hemin, physiabsorbed on C_8SH modified Au electrode *i.e.*, without the peptide scaffold, showed instant decay of the construct after the initial scan (Fig. S12, ESI†).
44 J. Rosenthal and D. G. Nocera, *Acc. Chem. Res.*, 2007, **40**, 543.
45 V. R. I. Kaila, M. I. Verkhovsky and M. r. Wikstrom, *Chem. Rev.*, 2010, **110**, 7062.